High-latitude stratospheric aerosol geoengineering can be more effective if injection is limited to spring

Walker Raymond Lee[1], Douglas G MacMartin[1], Daniele Visioni[2], and Ben Kravitz[3]

[1]Cornell University
[2]Sibley School of Mechanical and Aerospace Engineering, Cornell University
[3]Indiana University

November 21, 2022

Abstract

Stratospheric aerosol geoengineering focused on the Arctic could substantially reduce local and worldwide impacts of anthropogenic global warming. Because the Arctic receives little sunlight during the winter, stratospheric aerosols present in the winter at high latitudes have little impact on the climate, whereas stratospheric aerosols present during the summer achieve larger changes in radiative forcing. Injecting SO2 in the spring leads to peak aerosol optical depth (AOD) in the summer. We demonstrate that spring injection produces approximately twice as much summer AOD as year-round injection and restores approximately twice as much September sea ice, resulting in less increase in stratospheric sulfur burden, stratospheric heating, and stratospheric ozone depletion per unit of sea ice restored. We also find that differences in AOD between different seasonal injection strategies are small compared to the difference between annual and spring injection.

High-latitude stratospheric aerosol geoengineering can be more effective if injection is limited to spring

Walker Lee[1], **Douglas G. MacMartin**[1], **Daniele Visioni**[1], **Ben Kravitz**[2,3]

[1]Sibley School for Mechanical and Aerospace Engineering, Cornell University, Ithaca, NY, USA
[2]Department of Earth and Atmospheric Science, Indiana University, Bloomington, IN, USA
[3]Atmospheric Sciences and Global Change Division, Pacific Northwest National Laboratory, Richland, WA, USA

Key Points:

- Stratospheric aerosol geoengineering in the Arctic could reduce some impacts of climate change
- Aerosols present in summer reflect more light and therefore affect the climate more efficiently
- Our study shows that spring injections restore twice the summer sea ice as year round injections

Corresponding author: Walker Lee, `wl644@cornell.edu`

Abstract

Stratospheric aerosol geoengineering focused on the Arctic could substantially reduce local and worldwide impacts of anthropogenic global warming. Because the Arctic receives little sunlight during the winter, stratospheric aerosols present in the winter at high latitudes have little impact on the climate, whereas stratospheric aerosols present during the summer achieve larger changes in radiative forcing. Injecting SO_2 in the spring leads to peak aerosol optical depth (AOD) in the summer. We demonstrate that spring injection produces approximately twice as much summer AOD as year-round injection and restores approximately twice as much September sea ice, resulting in less increase in stratospheric sulfur burden, stratospheric heating, and stratospheric ozone depletion per unit of sea ice restored. We also find that differences in AOD between different seasonal injection strategies are small compared to the difference between annual and spring injection.

Plain Language Summary

Scattering small particles called aerosols into the sky - "geoengineering" - could reflect a small amount of sunlight in order to combat global warming. Doing this near the Arctic could help stop sea ice from melting, which would help preserve the Arctic climate. Our study shows that, for Arctic geoengineering, scattering particles in the spring is most efficient because the particles will be present throughout the summer, and the Arctic receives the most sunlight in the summer. Therefore, spring Arctic geoengineering could accomplish the same goals as year-round Arctic geoengineering, but with fewer particles and thus fewer negative side-effects.

1 Introduction

Arctic sea ice reflects solar radiation, regulates the exchange of energy and moisture between the ocean and the atmosphere, affects the thermohaline circulation and biogeochemistry of the Arctic, and serves as a habitat for ice-dwelling fauna (Meredith et al., 2019; D. Perovich et al., 2020; Barber et al., 2017). Since the beginning of the 21^{st} century, the Arctic has warmed more than twice as fast as the global average (Meredith et al., 2019; Ballinger et al., 2020), leading to decreases in the surface area and thickness of Arctic sea ice. The decline is largest during the annual minimum in September, where sea ice extent has been shrinking by an average of 83,000 km^2 per year, or 13% per decade (Meredith et al., 2019; D. Perovich et al., 2020; J. Stroeve & Notz, 2018). Increases in greenhouse gas (GHG) concentrations are the primary external driver for loss of sea ice in the Arctic (Kay et al., 2011; Notz & Marotzke, 2012; Fyfe et al., 2013), and this impact is likely underestimated by climate models (Notz & Stroeve, 2016). While climate models disagree on the exact rate of Arctic sea ice loss, they predict summer ice extent will drop below one million square kilometers by 2039-2045 regardless of emissions scenario (Snape & Forster, 2014) and that summer sea ice will eventually be lost in all shelf seas in all scenarios (Årthun et al., 2021). Projections of current trends suggest Arctic sea ice extent will wane more quickly than climate models predict, and that the Arctic may lose all of its September sea ice by 2035-2040 (Peng et al., 2018; J. Stroeve & Notz, 2018; Barber et al., 2017). Additionally, as the summer ice shelves retreat, a greater fraction of the Arctic is covered in young seasonal sea ice during the winter, which is thinner than multi-year sea ice and therefore more fragile and less reflective (D. Perovich et al., 2020; Barber et al., 2017; J. Stroeve & Notz, 2018; Meredith et al., 2019). This ice-albedo feedback further drives polar warming and Arctic amplification (Haine & Martin, 2017; Pithan & Mauritsen, 2014; D. K. Perovich & Polashenski, 2012; J. C. Stroeve et al., 2012); the ice-albedo feedback increased radiative heating in the Arctic Ocean by 6.4 Wm^{-2} between 1979 and 2014 (Pistone et al., 2014), resulting in 3-4 K of additional warming in the Arctic (Pithan & Mauritsen, 2014).

Mitigation of future CO_2 emissions alone may not be sufficient to prevent future climate impacts due to uncertainty in both the rate of future mitigation and in the climate response (Rogelj et al., 2016), and stratospheric aerosol injection (SAI) has been suggested as a possible temporary supplement to mitigation and carbon dioxide removal. There have been a number of simulations of "global" SAI strategies with the aim of maintaining a desired global mean temperature or other climate goals: the Geoengineering Large Ensemble (GLENS) study injected SO_2 at 30°N, 15°N, 15°S, and 30°S to try and stabilize global mean temperature alongside the interhemispheric and equator-to-pole temperature gradients (Kravitz et al., 2017; Tilmes et al., 2018), and the G3 and G4 experiments of the Geoengineering Model Intercomparison Project (GeoMIP) injected SO_2 above the equator to offset increases in radiative forcing and global mean temperature (Kravitz et al., 2011). Several studies have evaluated the Arctic impacts of these "global" approaches, finding that low- or mid-latitude injections of SO_2 could reduce global-warming-induced losses of sea ice and permafrost (Jiang et al., 2019; Lee et al., 2020; Moore et al., 2019; Chen et al., 2020). However, high-latitude SAI intended specifically to preserve the Arctic has been hypothesized to provide greater Arctic cooling per unit of injection than low-latitude SAI with smaller effects at low latitudes; for example, high-latitude injections have been shown to have smaller impacts on tropical precipitation than equatorial injections (Sun et al., 2020). Simulations of localized solar reduction northwards of 50, 60, and/or 70°N (or similar) have been shown to slow or reverse the loss of sea ice to varying extents (Caldeira & Wood, 2008; MacCracken et al., 2013; Tilmes et al., 2014; Kravitz et al., 2016). However, solar reduction is at best a limited proxy for SAI because it fails to account for stratospheric heating, changes to stratospheric ozone concentrations, changes to the stratospheric circulation, and perhaps most important of all, the actual spatial and seasonal distributions of AOD, which are driven by stratospheric transport (Visioni, MacMartin, & Kravitz, 2020). There have been a few studies of Arctic-focused SAI: Robock et al. (2008) injected 3 Mt/yr of SO_2 at 68°N, which restored SSI comparably to 5 Mt per year injected at the equator; Jackson et al. (2015) successfully managed the restoration and stabilization of SSI through injections at 78.55°N; and Sun et al. (2020) showed that aerosols present at high-latitudes injections have smaller impacts on tropical precipitation than equatorial injections.

There is substantial evidence that high-latitude SAI could, to some degree, counteract Arctic warming and consequent impacts on the Arctic more efficiently than low-latitude injection. However, to date, most simulated Arctic SAI strategies have been ad hoc; Jackson et al. (2015) and Lee et al. (2020) are the only strategies which have actively managed injection rates to maintain a desired SSI concentration, and Jackson et al. (2015) is the only strategy which has done so by injecting at a high latitude. Little effort has been undertaken to design an Arctic-focused SAI strategy: what combination of latitude, altitude, quantity, or timing of the injection will best preserve Arctic climate? Of these, time of year of injection is likely critical. Visioni, MacMartin, Kravitz, Richter, et al. (2020) found that injection in different seasons (at lower latitudes) has different regional climate outcomes. Moreover, the difference between injecting SO_2 year round, as has been the case for most simulations of SAI to date, and injecting seasonally, is likely even more critical for higher-latitude-injection Arctic-focused geoengineering due to both shorter aerosol lifetime and higher seasonality of insolation. Insolation north of 60°N is at least 10 times greater in summer than in winter (Peixoto & Oort, 1992); at low latitudes, insolation is comparable year-round, but at high latitudes, there is little to no sunlight in winter, meaning aerosols injected to reflect sunlight are largely useless. Furthermore, SO_2 injections are oxidized by OH, which forms in the presence of sunlight; since there is little to no sunlight in winter, SO_2 injected during the winter will oxidize into aerosols much more slowly, if at all. Finally, while sulfate aerosols present in winter oxidize more slowly and reflect less sunlight, interactions with other components of the atmosphere would still take place, including the trapping of longwave radiation, stratospheric ozone depletion, and sulfur deposition. Therefore, there is little purpose to injecting in winter, and aerosols should be concentrated in the summer for maximum effect. SO_2 injected in the spring will oxidize in time to be present as aerosols throughout the summer period of peak insolation (our results show an oxidation lifetime of approximately one month), producing greater effects on the climate than if the same quantity of SO_2 were distributed year-round. This hypothesis is supported by the results of Dai et al. (2018), who compared June and December injections of SO_2 and H_2SO_4 at 66.3°N; summer SO_2 injections produced 2-3 times greater maximum changes in radiative forcing than winter SO_2 injections, and summer H_2SO_4 injections (which do not need to oxidize and begin reflecting sunlight immediately) produced 3-5 times greater maximum changes in radiative forcing than winter H_2SO_4 injections. While Jackson et al. (2015) injected SO_2 seasonally, their primary focus was to determine whether sea ice was controllable rather than on the climate response, and they evaluated neither the differences relative to annually-constant injection nor the dependence on injection latitude and timing.

In this study, we directly compare year-round Arctic SAI with spring Arctic SAI to demonstrate that spring Arctic SAI restores more September sea ice (SSI) per unit of SO_2 injected; additionally, spring Arctic SAI results in less stratospheric sulfur burden, heating, and ozone depletion per unit of SSI restored. We also explore the design space of seasonal Arctic SAI by comparing the AOD of several different strategies; we do this by modifying the latitude, timing, and duration of injection while keeping the total injection per year constant. In Section 2, we describe our climate model and our simulations. We present our results in Section 3, and in Section 4 we discuss our results and their implications on future geoengineering research.

2 Climate Model and Simulations

In this study, we present simulations of six new stratospheric aerosol injection strategies. Each simulation begins in the year 2030 and uses the RCP8.5 warming scenario. In each case, we inject a total of 12 Tg of SO_2 every year at an altitude of 14.7-14.9 km at a single prescribed latitude. Simulation specifications are described in Table 1. Our two primary simulations each run for 10 years and compare a seasonal injection strategy to a year-round strategy, both injecting at 60°N. In addition, we conducted four 5-year simulations to evaluate the effects of timing or latitude of injection. We choose 60°N as the injection latitude for our primary simulations because we wish to inject north of the stratospheric polar vortex that acts as a transport barrier for the aerosols (Visioni, MacMartin, Kravitz, Lee, et al., 2020), but also as far south as possible so as to maximize the surface area covered by the aerosols as they are transported northward; this choice is also supported by the results of MacCracken et al. (2013) and Tilmes et al. (2014), in which solar reductions poleward of 60°N or thereabouts gave the largest restoration of SSI.

Our strategies were simulated using the Community Earth System Model version 1 with the Whole Atmosphere Community Climate Model as the atmospheric component, denoted CESM1(WACCM), and is fully coupled with the Parallel Ocean Program (POP2) ocean, Community Land Model (CLM)4.5 land, and the Community Ice CodE (CICE)4 ice components ("CICE: the Los Alamos Sea Ice Model Documentation and Software User's Manual", 2010; WANG et al., 2020). CICE is one of the most widely used models to simulate the growth, melting and movement of Arctic sea ice, for operational forecasts and to understand sea-ice processes, and has been thoroughly validated (Roberts et al., 2018; DuVivier et al., 2020) both in its stand-alone form and coupled with CESM. CESM was run at a horizontal resolution of 0.9 degrees latitude by 1.25 degrees longitude, and WACCM uses a 70-layer vertical grid with a maximum altitude of 145 km, approximately 10-6 hPa. The model used the modal aerosol component MAM3 (Liu et al., 2012), which uses a three-bin distribution, and is fully coupled to radiation and atmospheric chemistry. The atmospheric model has been validated against observations both in quiescent conditions and in the aftermath of explosive volcanic eruptions (Mills et al.,

Table 1. Parameters for the six simulations presented in this study. All simulations begin in 2030; simulations are named after the time of year in which they inject SO_2 and the latitude at which they inject. All simulations inject 12 Tg SO_2/year, which is distributed evenly among the months of injection.

Simulation	Length	SO_2/yr	Inj. Months[a]	SO_2/month	Inj. Latitude
MAM-60	10 years	12 Tg	MAM	4 Tg	60°N
ANN-60	10 years	12 Tg	all	1 Tg	60°N
MAM-67.5	5 years	12 Tg	MAM	4 Tg	67.5°N
MAM-75	5 years	12 Tg	MAM	4 Tg	75°N
AM-60	5 years	12 Tg	AM	6 Tg	60°N
AMJ-60	5 years	12 Tg	AMJ	4 Tg	60°N

[a]MAM = March, April, and May; AM = April and May; AMJ = April, May, and June.

2016, 2017) and is reasonably consistent with observations of, amongst other things, stratospheric ozone evolution and polar stratospheric clouds formation (Tilmes et al., 2018 - JGR, not BAMS) and their interaction with surface climate (Harari et al., 2019); it has also been used extensively for studying stratospheric aerosol geoengineering (Kravitz et al., 2017; Tilmes et al., 2018; Visioni, MacMartin, Kravitz, Richter, et al., 2020; Lee et al., 2020).

3 Results

In Figure 1, we present the seasonal cycle of stratospheric aerosol optical depth (AOD) for all simulations. AOD for all spring injection cases peaks in the summer months, and all spring injections achieve a peak AOD approximately 2.5 times greater than that of ANN-60 regardless of the timing or latitude of injection. For all MAM injections, this peak occurs in June; for AMJ, the peak occurs in July, and for AM, June and July are comparable. For MAM-60, we compute an oxidation timescale of approximately four weeks based on the decay rates of stratospheric SO_2, which is consistent with the peak AOD occurring one month after injection stops. All spring injections at 60°N have comparable annual mean AOD profiles, regardless of injection timing. MAM-67.5 produces more AOD than MAM-60 everywhere in the Northern Hemisphere and averages 20% more AOD at high latitudes; spring injections at 67.5°N might therefore be even more efficient than spring injections at 60°N at restoring SSI, but these differences are small compared to the difference between either of them and annually constant injection. Annual mean AOD for spring injections is higher than that of year-round injection in all latitudes north of the equator, regardless of injection latitude or timing. As could be expected, seasonal variations in Arctic AOD are significantly larger for spring injection than for year-round injection, but ANN-60 Arctic AOD is still higher in summer than in winter due to lower production of OH through photolysis of O_3 in the winter and subsequently reduced oxidation of SO_2. Even though ANN-60 injects in the autumn and winter, winter AOD for ANN-60 in the Arctic is comparable to those of spring injections; in December, January, and February, the average AOD north of 60°N for ANN-60 is 0.13, while the other simulations range from 0.09 (MAM-60) to 0.14 (MAM-67.5). Lastly, we observe that while changes in AOD are largest in the Arctic, they are not confined to the Arctic; AOD produced by injections at 60°N extends to the mid-latitudes in all seasons for year-round injection and into the tropics in the summer for MAM-60. Additional comparisons to the AOD of seasonal injections at 30°N and 45°N can be found in the supplementary material.

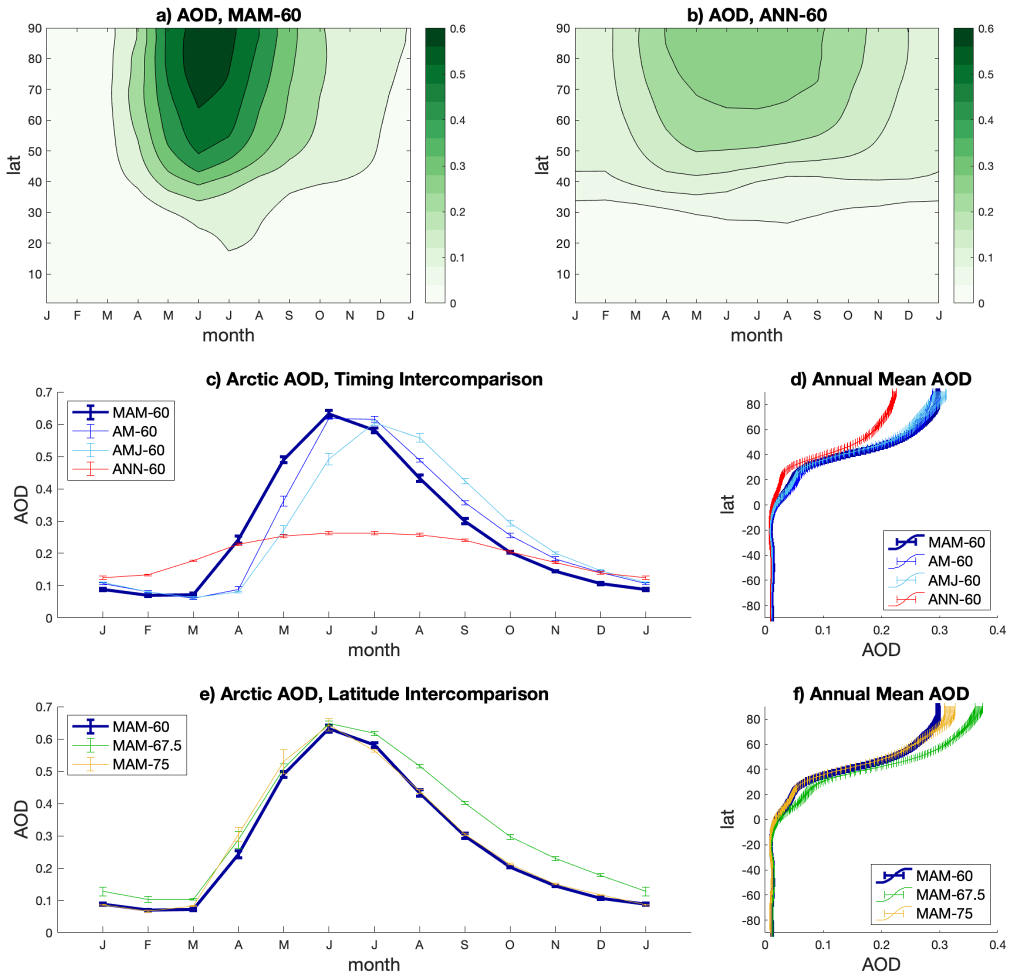

Figure 1. AOD for all simulations. Figures 1a and 1b (top row) plot the seasonal cycles of AOD for MAM-60 (left) and ANN-60 (right) as a function of latitude. Figures 1c and 1d (middle row) compare different injection timings, and Figures 1e and 1f (bottom row) compares different injection latitudes; the left panels plot seasonal cycles of Arctic AOD, and the right panels plot annual mean zonal mean AOD as a function of latitude. MAM-60 and ANN-60 data are averaged over the last 5 years of simulation; data from the other simulations are averaged over the last 3 years as in Visioni, MacMartin, Kravitz, Richter, et al. (2020).

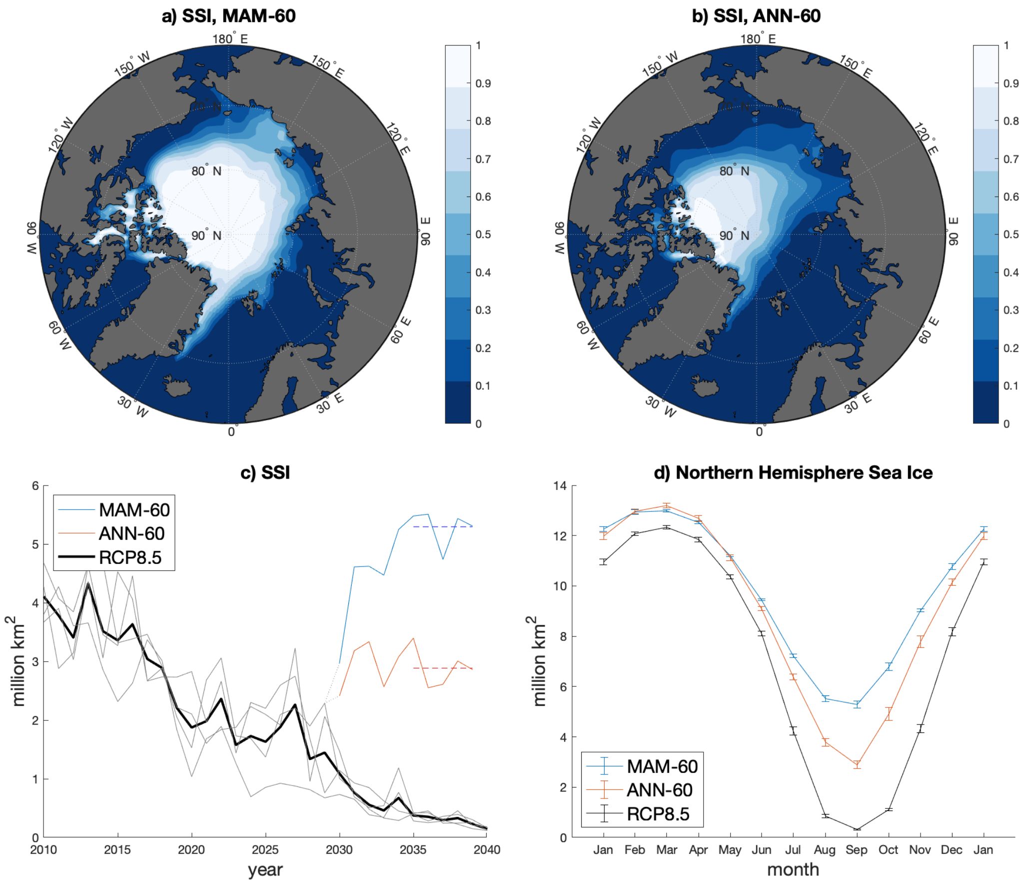

Figure 2. Comparison of sea ice between MAM-60 and ANN-60. Figures 2a and 2b (top) show the extent of September Sea Ice (SSI) averaged over the last five years of simulation for each strategy; the color scale denotes the fraction of each grid cell covered in ice. Figure 2c (bottom left) plots SSI over time for both strategies alongside RCP8.5. The thick black line denotes the RCP8.5 ensemble average, while faint black lines denote individual ensemble members; dotted lines connect the blue and red MAM-60 and ANN-60 lines to the ensemble member from which they branched. Horizontal blue and red dashed lines denote the average SSI of MAM-60 and ANN-60, respectively, over the last five years of simulation. Figure 2d (bottom right) plots the seasonal cycle of sea ice for each simulation and for RCP8.5, averaged over the last five years of simulation.

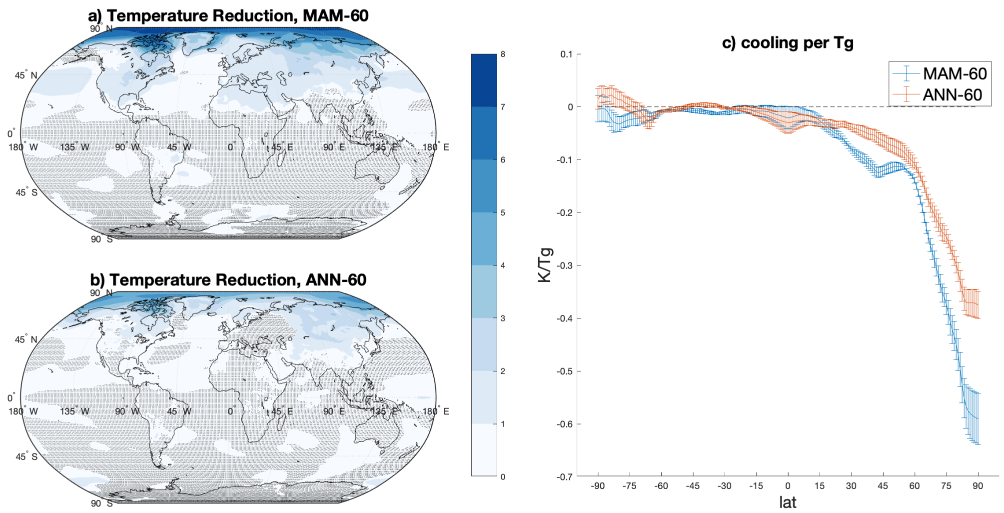

Figure 3. Temperature comparison between MAM-60 and ANN-60, averaged over the last five years of simulation, relative to RCP8.5 during the same period (2035-2039). Figures 3a and 3b (left) plots the temperature decrease relative to RCP8.5; gray shading indicates areas where temperature distributions are statistically identical ($\alpha = 0.5$). Figure 3c (right) shows the temperature difference from RCP8.5 as a function of latitude, normalized by injection quantity (12 Tg/yr).

Figure 2 shows the behavior of sea ice for MAM-60 and ANN-60, along with RCP.85 for comparison. Under RCP8.5, the average SSI in 2035-2039 is 0.32±0.02 million km^2, where ± value indicates standard error. For ANN-60, this value is 2.9±0.2 million km^2, a restoration of 2.6 million km^2; for MAM-60, this value is 5.3±0.1 million km^2, a restoration of 5.0 million km^2, approximately twice as much. Sea ice extents for MAM-60 and ANN-60 are comparable in the winter. SSI in MAM-60 relative to ANN-60 is both increased in concentration near the pole as well as extending further from the pole.

Figure 3 shows the change in temperature for MAM-60 and ANN-60 relative to RCP8.5 during the same time period (2035-2039). Temperature changes for both simulations are largest in the Arctic but are not confined to the Arctic; Fig. 3a and 3b show statistically significant changes for ANN-60 in large parts of Asia and parts of North America and for MAM-60 in most of the Northern Hemisphere. The average temperature changes north of 60N for MAM-60 and ANN-60 are -3.7 ± 0.2 K and -2.5 ± 0.2 K, respectively; the global mean temperature changes for MAM-60 and ANN-60 are -0.65 ± 0.06 K and -0.44 ± 0.06 K, respectively, a factor of approximately 1.5 for both metrics.

In addition to surface cooling, stratospheric sulfate aerosols will warm the stratosphere (Ferraro et al., 2015) and contribute to high-latitude ozone loss (Robrecht et al., 2020). In Figure 4, we present annual mean increases in stratospheric sulfate mixing ratio and its effect on air temperature and ozone concentration for MAM-60 and ANN-60; all the changes are normalized by the extent of SSI restored. This way we can evaluate the effects of both strategies based on their efficacy: in this case MAM-60 produces smaller changes than ANN-60, and the effects are also more localized. In ANN-60, more aerosols are transported equatorward, and aerosols are also present at high latitudes year-round. We observe a stratospheric heating peak over the North Pole, as a possible consequence of both ozone destruction in early spring and the aerosols absorbing more planetary radiation in the winter months. Additionally, ANN-60 shows some ozone increase

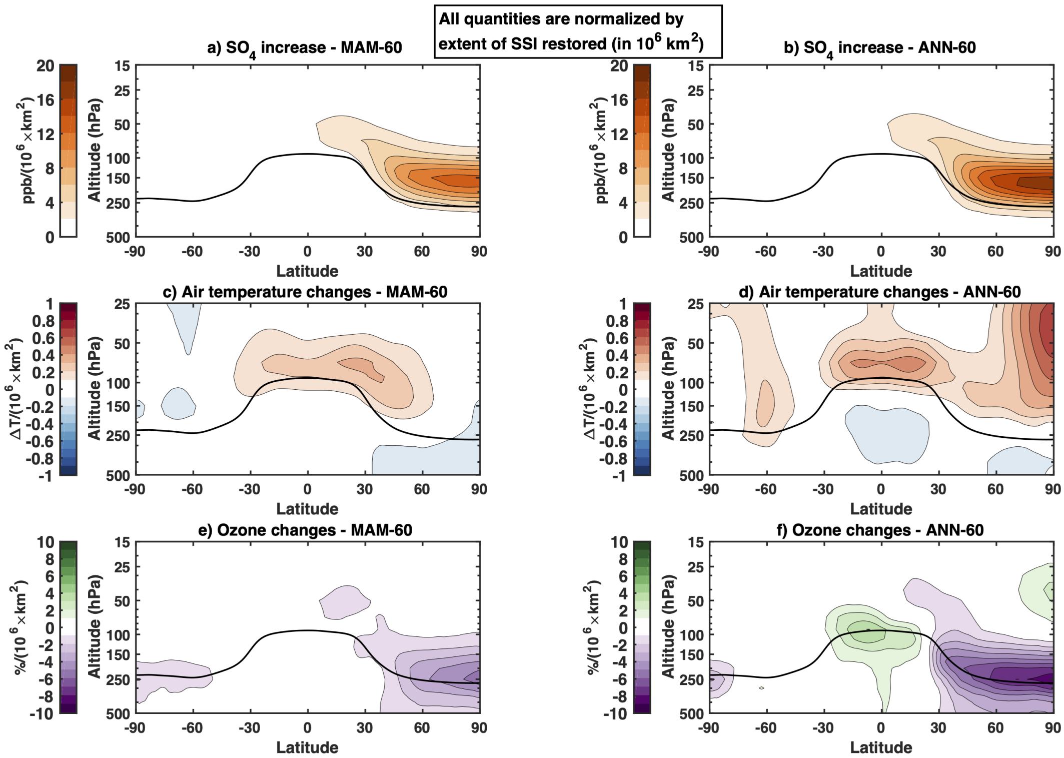

Figure 4. Changes to atmospheric temperature and chemical composition as functions of latitude and altitude for MAM-60 (left) and ANN-60 (right), relative to RCP8.5 during the same period (2035-2039). Figures 4a and 4b (top) plot changes to SO_4 mixing ratio, Figures 4c and 4d (middle) plot temperature change, and Figures 4e and 4f (bottom) plot changes to ozone concentration. All changes are averaged over the last five years of simulation and normalized by the average extent of SSI restored relative to RCP8.5.

in the upper troposphere-lowermost stratosphere near the equator, and further stratospheric ozone destruction over the Arctic compared with MAM-60.

One of the expected changes from focusing a geoengineered cooling over the Arctic would be an increase in meridional heat transport (Tilmes et al., 2014), and consequent shifts in tropical precipitation (Robock et al., 2008; MacCracken et al., 2013; Kravitz et al., 2016). Changes to meridional heat transport at 60°N are small for both MAM-60 and ANN-60. The total meridional heat flux at 60°N under RCP8.5 in the years 2035-2039 (computed by the top-of-atmosphere radiation balance as in Wunsch (2005)) is 3.41 $\pm$ 0.01 PW; ANN-60 shows no statistically detectable change, while MAM-60 shows a slight increase to 3.45 $\pm$ 0.01 PW. Both MAM-60 and ANN-60 show detectable changes to tropical heat transport. We define the ITCZ as the latitude of zero meridional heat transport, as in Byrne et al. (2018); by fitting a linear function to meridional heat transport as a function of latitude between 10°S and 10°N and solving for the intercept, we compute an ITCZ located at -2.4 $\pm$ 0.1 degrees latitude for RCP8.5. ANN-60 pushes the ITCZ south to -2.9 $\pm$ 0.1 degrees, and MAM-60 shifts the ITCZ further to -3.4 $\pm$ 0.1 degrees, approximately a factor of two; this is consistent with the understanding that SAI in one hemisphere pushes the ITCZ towards the other hemisphere (Haywood et al., 2013). This change in ITCZ likely impacts tropical precipitation, but computing the tropical precipitation centroid from 20°S to 20°N as in Lee et al 2020 shows no statistically significant change from RCP8.5. Comparisons of SSI extent, temperature, heat transport, and tropical precipitation values for RCP8.5, MAM-60, and ANN-60 can be found in the supplementary material.

4 Discussion and Conclusions

In this study, we directly compare simulations of year-round and spring SAI in the Arctic. Per teragram of SO_2 injected, spring injection at 60°N restores approximately twice as much SSI and achieves approximately 1.5 times the Arctic and global mean temperature reductions as year-round injection. Assuming that the climate responds approximately linearly to small changes in radiative forcing, spring injection could achieve similar climate goals to year-round injection with one-half to two-thirds the injection quantity, resulting in smaller increases to stratospheric sulfur burden, stratospheric heating, and stratospheric ozone depletion, as well as less surface acid rain deposition (Visioni, Slessarev, et al., 2020).

The primary focus of this study is the efficacy of seasonal versus year-round SAI in preserving SSI; we only look at a few of the relevant impacts, and we do so in only one climate model. In order to support informed future decisions around SAI in general and Arctic-focused SAI in particular, a much more careful evaluation of multiple different climate impacts would be necessary, especially considering the interconnectedness of the Arctic climate: Greenland ice sheet melt is strongly influenced by any changes in cloud cover (Hofer et al., 2017), permafrost thaw is affected by changes in snow depth that provide insulation, etc. A model intercomparison would also be critical to understand confidence. Furthermore, while it is clear from our results that the biggest impact on efficiency arises from focusing injection in the spring, there is more work that needs to be done to better understand trade-offs with injection altitude, latitude, and timing. The different AOD seasonal cycles of MAM-60, AM-60, and AMJ-60 demonstrate that we can change the timing of the AOD peak; while the peak AOD of MAM-60 coincides with peak insolation in June, there is more reflective sea ice then than there is later in the year, and so the detailed relationship between the injection timing or duration and sea ice recovery is not obvious and likely depends on the extent of summer sea ice remaining in a given year. Additionally, depending on the objectives of a hypothetical future geoengineering deployment, it may be useful to consider injecting at multiple different latitudes simultaneously to manage different goals. For example, SAI in one hemisphere pushes the ITCZ towards the other hemisphere (Sun et al., 2020), so another injection at 60°S or other latitudes in the Southern Hemisphere could counteract the effects of Arctic SAI on low-latitude heat transport as proposed by MacCracken et al (2014) and Kravitz et al. (2016). Finally, we note that in contrast to more "globally" focused strategies that have been the focus of almost all modeling work, as well as the context motivating most governance studies, Arctic-focused SAI could be deployed without the development of new aircraft capability. Combined with potential concerns over climate change in the Arctic, it is plausible that Arctic-focused SAI may be more likely to be deployed, and sooner, than any global SAI strategy.

Acknowledgments

We would like to acknowledge high-performance computing support from Cheyenne (doi:10.5065/D6RX99HX) provided by NCAR's Computational and Information Systems Laboratory, sponsored by the National Science Foundation. Support for WL and DM was provided by the National Science Foundation through agreement CBET-1818759. Support for DV was provided by the Atkinson Center for a Sustainable Future at Cornell University. Support for BK was provided in part by the National Sciences Foundation through agreement CBET-1931641, the Indiana University Environmental Resilience Institute, and the *Prepared for Environmental Change* Grand Challenge initiative. The Pacific Northwest National Laboratory is operated for the U.S. Department of Energy by Battelle Memorial Institute under contract DE-AC05-76RL01830. The CESM project is supported primarily by the National Science Foundation. This work was supported by the National Center for Atmospheric Research, which is a major facility sponsored by the National Science Foundation under Cooperative Agreement No. 1852977. Data will be made available online through the Cornell e-Commons Library.

References

Ballinger, T. J., Overland, J. E., Wang, M., Bhatt, U. S., Hanna, E., Hanssen-Bauer, I., ... Walsh, J. E. (2020). *Arctic report card 2020: Surface air temperature.* Retrieved from `https://www.arctic.noaa.gov/Report-Card/Report-Card-2020/ArtMID/7975/ArticleID/878/Surface-Air-Temperature` doi: DOI:10.25923/gcw8-2z06

Barber, D. G., Meier, W. N., Gerland, S., Mundy, C., Holland, M., Kern, S., ... Tamura, T. (2017). *Snow, water, ice and permafrost in the arctic (swipa) 2017: Arctic sea ice.* Retrieved from `https://www.amap.no/documents/download/2987/inline`

Byrne, M. P., Pendergrass, A. G., Rapp, A. D., & Wodzicki, K. R. (2018). Response of the intertropical convergence zone to climate change: Location, width, and strength. *Current Climate Change Reports*, *4*, 355–370. Retrieved from `https://link.springer.com/article/10.1007/s40641-018-0110-5` doi: https://doi.org/10.1007/s40641-018-0110-5

Caldeira, K., & Wood, L. (2008). Global and arctic climate engineering: numerical model studies. *Philosophical Transactions of the Royal Society A: Mathematical, Physical and Engineering Sciences*, *366*(1882), 4039-4056. Retrieved from `https://royalsocietypublishing.org/doi/abs/10.1098/rsta.2008.0132` doi: 10.1098/rsta.2008.0132

Chen, Y., Liu, A., & Moore, J. C. (2020). Mitigation of arctic permafrost carbon loss through stratospheric aerosol geoengineering. *Nature Communications*, *11*(2430). Retrieved from `https://www.nature.com/articles/s41467-020-16357-8` doi: https://doi.org/10.1038/s41467-020-16357-8

Cice: the los alamos sea ice model documentation and software user's manual [Computer software manual]. (2010). Los Alamos NM 87545. Retrieved from `https://csdms.colorado.edu/w/images/CICE_documentation_and_software_user\%27s_manual.pdf`

Dai, Z., Weisenstein, D. K., & Keith, D. W. (2018). Tailoring meridional and seasonal radiative forcing by sulfate aerosol solar geoengineering. *Geophysical Research Letters*, *45*(2), 1030-1039. Retrieved from `https://agupubs.onlinelibrary.wiley.com/doi/abs/10.1002/2017GL076472` doi: 10.1002/2017GL076472

DuVivier, A. K., DeRepentigny, P., Holland, M. M., Webster, M., Kay, J. E., & Perovich, D. (2020). Going with the floe: tracking cesm large ensemble sea ice in the arctic provides context for ship-based observations. *The Cryosphere*, *14*(4), 1259–1271. Retrieved from `https://tc.copernicus.org/articles/14/1259/2020/` doi: 10.5194/tc-14-1259-2020

Ferraro, A. J., Charlton-Perez, A. J., & Highwood, E. J. (2015). Stratospheric dynamics and midlatitude jets under geoengineering with space mirrors and sulfate and titania aerosols. *Journal of Geophysical Research: Atmospheres*, *120*(2), 414-429. Retrieved from `https://agupubs.onlinelibrary.wiley.com/doi/abs/10.1002/2014JD022734` doi: https://doi.org/10.1002/2014JD022734

Fyfe, J. C., von Salzen, K., Gillett, N. P., Arora, V. K., Flato, G. M., & McConnell, J. R. (2013). One hundred years of arctic surface temperature variation due to anthropogenic influence. *Scientific Reports*, *3*(2645). Retrieved from `https://www.nature.com/articles/srep02645` doi: https://doi.org/10.1038/srep02645

Haine, T. W. N., & Martin, T. (2017). The arctic-subarctic sea ice system is entering a seasonal regime: Implications for future arctic amplification. *Scientific Reports*, *7*(4618). Retrieved from `https://www.nature.com/articles/s41598-017-04573-0` doi: https://doi.org/10.1038/s41598-017-04573-0

Harari, O., Garfinkel, C. I., Ziskin Ziv, S., Morgenstern, O., Zeng, G., Tilmes, S., . . . Davis, S. (2019). Influence of arctic stratospheric ozone on surface climate in ccmi models. *Atmospheric Chemistry and Physics*, *19*(14), 9253–9268. Retrieved from `https://acp.copernicus.org/articles/19/9253/2019/` doi: 10.5194/acp-19-9253-2019

Haywood, J. M., Jones, A., Bellouin, N., & Stephenson, D. (2013). Asymmetric forcing from stratospheric aerosols impacts Sahelian rainfall. *Nature Climate Change*, *3*, 660–665. Retrieved from `https://doi.org/10.1038/nclimate1857` (doi:10.1038/nclimate1857) doi: 10.1038/nclimate1857

Hofer, S., Tedstone, A. J., Fettweis, X., & Bamber, J. L. (2017). Decreasing cloud cover drives the recent mass loss on the greenland ice sheet. *Science Advances*, *3*(6). Retrieved from `https://advances.sciencemag.org/content/3/6/e1700584` doi: 10.1126/sciadv.1700584

Jackson, L. S., Crook, J. A., Jarvis, A., Leedal, D., Ridgwell, A., Vaughan, N., & Forster, P. M. (2015). Assessing the controllability of arctic sea ice extent by sulfate aerosol geoengineering. *Geophysical Research Letters*, *42*(4), 1223-1231. Retrieved from `https://agupubs.onlinelibrary.wiley.com/doi/abs/10.1002/2014GL062240` doi: 10.1002/2014GL062240

Jiang, J., Cao, L., MacMartin, D. G., Simpson, I. R., Kravitz, B., Cheng, W., . . . Mills, M. J. (2019). Stratospheric sulfate aerosol geoengineering could alter the high-latitude seasonal cycle. *Geophysical Research Letters*, *46*(23), 14153-14163. Retrieved from `https://agupubs.onlinelibrary.wiley.com/doi/abs/10.1029/2019GL085758` doi: 10.1029/2019GL085758

Kay, J. E., Holland, M. M., & Jahn, A. (2011). Inter-annual to multi-decadal arctic sea ice extent trends in a warming world. *Geophysical Research Letters*, *38*(15). Retrieved from `https://agupubs.onlinelibrary.wiley.com/doi/abs/10.1029/2011GL048008` doi: https://doi.org/10.1029/2011GL048008

Kravitz, B., Macmartin, D., Wang, H., & Rasch, P. (2016, 05). Geoengineering as a design problem. *Earth System Dynamics*, *7*, 469-497. doi: 10.5194/esd-7-469-2016

Kravitz, B., MacMartin, D. G., Mills, M. J., Richter, J. H., Tilmes, S., Lamarque, J.-F., … Vitt, F. (2017). First simulations of designing stratospheric sulfate aerosol geoengineering to meet multiple simultaneous climate objectives. *Journal of Geophysical Research: Atmospheres*, *122*(23), 12,616-12,634. Retrieved from https://agupubs.onlinelibrary.wiley.com/doi/abs/10.1002/2017JD026874 doi: 10.1002/2017JD026874

Kravitz, B., Robock, A., Boucher, O., Schmidt, H., Taylor, K. E., Stenchikov, G., & Schulz, M. (2011). The geoengineering model intercomparison project (geomip). *Atmospheric Science Letters*, *12*(2), 162-167. Retrieved from https://rmets.onlinelibrary.wiley.com/doi/abs/10.1002/asl.316 doi: https://doi.org/10.1002/asl.316

Lee, W., MacMartin, D., Visioni, D., & Kravitz, B. (2020). Expanding the design space of stratospheric aerosol geoengineering to include precipitation-based objectives and explore trade-offs. *Earth System Dynamics*, *11*(4), 1051–1072. Retrieved from https://esd.copernicus.org/articles/11/1051/2020/ doi: 10.5194/esd-11-1051-2020

Liu, X., Easter, R. C., Ghan, S. J., Zaveri, R., Rasch, P., Shi, X., … Mitchell, D. (2012). Toward a minimal representation of aerosols in climate models: description and evaluation in the community atmosphere model cam5. *Geoscientific Model Development*, *5*(3), 709–739. Retrieved from https://gmd.copernicus.org/articles/5/709/2012/ doi: 10.5194/gmd-5-709-2012

MacCracken, M., Shin, H.-J., Caldeira, K., & Ban-Weiss, G. (2013, 09). Climate response to imposed solar radiation reductions in high latitudes. *Earth System Dynamics*, *4*. doi: 10.5194/esd-4-301-2013

Meredith, M., Sommerkorn, M., Cassotta, S., Derksen, C., Ekaykin, A., Hollowed, A., … Schuur, E. (2019). *Ipcc special report on the ocean and cryosphere in a changing climate: Polar regions* (H.-O. Pörtner et al., Eds.). Retrieved from https://www.ipcc.ch/srocc/

Mills, M. J., Richter, J. H., Tilmes, S., Kravitz, B., MacMartin, D. G., Glanville, A. A., … Kinnison, D. E. (2017). Radiative and chemical response to interactive stratospheric sulfate aerosols in fully coupled cesm1(waccm). *Journal of Geophysical Research: Atmospheres*, *122*(23), 13,061-13,078. Retrieved from https://agupubs.onlinelibrary.wiley.com/doi/abs/10.1002/2017JD027006 doi: 10.1002/2017JD027006

Mills, M. J., Schmidt, A., Easter, R., Solomon, S., Kinnison, D. E., Ghan, S. J., … Gettelman, A. (2016). Global volcanic aerosol properties derived from emissions, 1990–2014, using cesm1(waccm). *Journal of Geophysical Research: Atmospheres*, *121*(5), 2332-2348. Retrieved from https://agupubs.onlinelibrary.wiley.com/doi/abs/10.1002/2015JD024290 doi: 10.1002/2015JD024290

Moore, J. C., Yue, C., Zhao, L., Guo, X., Watanabe, S., & Ji, D. (2019). Greenland ice sheet response to stratospheric aerosol injection geoengineering. *Earth's Future*, *7*(12), 1451-1463. Retrieved from https://agupubs.onlinelibrary.wiley.com/doi/abs/10.1029/2019EF001393 doi: https://doi.org/10.1029/2019EF001393

Notz, D., & Marotzke, J. (2012). Observations reveal external driver for arctic sea-ice retreat. *Geophysical Research Letters*, *39*(8). Retrieved from https://agupubs.onlinelibrary.wiley.com/doi/abs/10.1029/2012GL051094 doi: https://doi.org/10.1029/2012GL051094

Notz, D., & Stroeve, J. (2016). Observed arctic sea-ice loss directly follows anthropogenic co2 emission. *Science*, *354*(6313), 747–750. Retrieved from https://science.sciencemag.org/content/354/6313/747 doi: 10.1126/science.aag2345

Peixoto, J. P., & Oort, A. H. (1992). *Physics of climate* (1st ed.). AIP-Press.

Peng, G., Steele, M., Bliss, A. C., Meier, W. N., & Dickinson, S. (2018). Temporal means and variability of arctic sea ice melt and freeze season climate indicators using a satellite climate data record. *Remote Sensing*, *10*(9). Retrieved from `https://www.mdpi.com/2072-4292/10/9/1328` doi: 10.3390/rs10091328

Perovich, D., Meier, W., Tschudi, M., Hendricks, S., Petty, A. A., Divine, D., ... Wood, K. (2020). *Arctic report card 2020: Sea ice.* Retrieved from `https://arctic.noaa.gov/Report-Card/Report-Card-2020/ArtMID/7975/ArticleID/891/Sea-Ice` doi: 10.25923/n170-9h57

Perovich, D. K., & Polashenski, C. (2012). Albedo evolution of seasonal arctic sea ice. *Geophysical Research Letters*, *39*(8). Retrieved from `https://agupubs.onlinelibrary.wiley.com/doi/abs/10.1029/2012GL051432` doi: https://doi.org/10.1029/2012GL051432

Pistone, K., Eisenman, I., & Ramanathan, V. (2014). Observational determination of albedo decrease caused by vanishing arctic sea ice. *Proceedings of the National Academy of Sciences*, *111*(9), 3322–3326. Retrieved from `https://www.pnas.org/content/111/9/3322` doi: 10.1073/pnas.1318201111

Pithan, F., & Mauritsen, T. (2014). Arctic amplification dominated by temperature feedbacks in contemporary climate models. *Nature Geoscience*, *7*, 181–184. Retrieved from `https://www.nature.com/articles/ngeo2071` doi: https://doi.org/10.1038/ngeo2071

Roberts, A. F., Hunke, E. C., Allard, R., Bailey, D. A., Craig, A. P., Lemieux, J.-F., & Turner, M. D. (2018). Quality control for community-based sea-ice model development. *Philosophical Transactions of the Royal Society A: Mathematical, Physical and Engineering Sciences*, *376*(2129), 20170344. Retrieved from `https://royalsocietypublishing.org/doi/abs/10.1098/rsta.2017.0344` doi: 10.1098/rsta.2017.0344

Robock, A., Oman, L., & Stenchikov, G. L. (2008). Regional climate responses to geoengineering with tropical and arctic so2 injections. *Journal of Geophysical Research: Atmospheres*, *113*(D16). Retrieved from `https://agupubs.onlinelibrary.wiley.com/doi/abs/10.1029/2008JD010050` doi: 10.1029/2008JD010050

Robrecht, S., Vogel, B., Tilmes, S., & Müller, R. (2020). Potential of future stratospheric ozone loss in the mid-latitudes under climate change and sulfate geoengineering. *Atmospheric Chemistry and Physics Discussions*, *2020*, 1–40. Retrieved from `https://acp.copernicus.org/preprints/acp-2020-747/` doi: 10.5194/acp-2020-747

Rogelj, J., den Elzen, M., Höhne, N., Fransen, T., Fekete, H., Winkler, H., ... Meinshausen, M. (2016). Paris agreement climate proposals need a boost to keep warming well below 2°c. *Nature*, *534*, 631-–639. Retrieved from `https://www.nature.com/articles/nature18307` doi: https://doi.org/10.1038/nature18307

Snape, T. J., & Forster, P. M. (2014). Decline of arctic sea ice: Evaluation and weighting of cmip5 projections. *Journal of Geophysical Research: Atmospheres*, *119*(2), 546-554. Retrieved from `https://agupubs.onlinelibrary.wiley.com/doi/abs/10.1002/2013JD020593` doi: https://doi.org/10.1002/2013JD020593

Stroeve, J., & Notz, D. (2018, sep). Changing state of arctic sea ice across all seasons. *Environmental Research Letters*, *13*(10), 103001. Retrieved from `https://doi.org/10.1088/1748-9326/aade56` doi: 10.1088/1748-9326/aade56

Stroeve, J. C., Serreze, M. C., Holland, M. M., Kay, J. E., Malanik, J., & Barrett, A. P. (2012). The arctic's rapidly shrinking sea ice cover: a research synthesis. *Climatic Change*, *110*, 1005—1027. Retrieved from `https://link.springer.com/article/10.1007/s10584-011-0101-1` doi: https://doi.org/10.1007/s10584-011-0101-1

Sun, W., Wang, B., Chen, D., Gao, C., Lu, G., & Liu, J. (2020). Global monsoon response to tropical and arctic stratospheric aerosol injection. *Climate Dynamics*, *55*, 2107—2121. Retrieved from `https://link.springer.com/article/10.1007/s00382-020-05371-7` doi: https://doi.org/10.1007/s00382-020-05371-7

Tilmes, S., Jahn, A., Kay, J. E., Holland, M., & Lamarque, J.-F. (2014). Can regional climate engineering save the summer arctic sea ice? *Geophysical Research Letters*, *41*(3), 880-885. Retrieved from `https://agupubs.onlinelibrary.wiley.com/doi/abs/10.1002/2013GL058731` doi: https://doi.org/10.1002/2013GL058731

Tilmes, S., Richter, J. H., Kravitz, B., MacMartin, D. G., Mills, M. J., Simpson, I. R., … Ghosh, S. (2018, 12). CESM1(WACCM) Stratospheric Aerosol Geoengineering Large Ensemble Project. *Bulletin of the American Meteorological Society*, *99*(11), 2361-2371. Retrieved from `https://doi.org/10.1175/BAMS-D-17-0267.1` doi: 10.1175/BAMS-D-17-0267.1

Visioni, D., MacMartin, D. G., & Kravitz, B. (2020). Is turning down the sun a good proxy for stratospheric sulfate geoengineering? *Earth and Space Science Open Archive*, 50. Retrieved from `https://doi.org/10.1002/essoar.10504448.1` doi: 10.1002/essoar.10504448.1

Visioni, D., MacMartin, D. G., Kravitz, B., Lee, W., Simpson, I. R., & Richter, J. H. (2020). Reduced poleward transport due to stratospheric heating under stratospheric aerosols geoengineering. *Geophysical Research Letters*, *47*(17), e2020GL089470. Retrieved from `https://agupubs.onlinelibrary.wiley.com/doi/abs/10.1029/2020GL089470` (e2020GL089470 10.1029/2020GL089470) doi: 10.1029/2020GL089470

Visioni, D., MacMartin, D. G., Kravitz, B., Richter, J. H., Tilmes, S., & Mills, M. J. (2020). Seasonally modulated stratospheric aerosol geoengineering alters the climate outcomes. *Geophysical Research Letters*, *47*(12), e2020GL088337. Retrieved from `https://agupubs.onlinelibrary.wiley.com/doi/abs/10.1029/2020GL088337` (e2020GL088337 2020GL088337) doi: 10.1029/2020GL088337

Visioni, D., Slessarev, E., MacMartin, D. G., Mahowald, N. M., Goodale, C. L., & Xia, L. (2020, sep). What goes up must come down: impacts of deposition in a sulfate geoengineering scenario. *Environmental Research Letters*, *15*(9), 094063. Retrieved from `https://doi.org/10.1088/1748-9326/ab94eb` doi: 10.1088/1748-9326/ab94eb

WANG, H., ZHANG, L., CHU, M., & HU, S. (2020). Advantages of the latest los alamos sea-ice model (cice): evaluation of the simulated spatiotemporal variation of arctic sea ice. *Atmospheric and Oceanic Science Letters*, *13*(2), 113-120. Retrieved from `https://doi.org/10.1080/16742834.2020.1712186` doi: 10.1080/16742834.2020.1712186

Wunsch, C. (2005). The total meridional heat flux and its oceanic and atmospheric partition. *Journal of Climate*, *18*(21), 4374 - 4380. Retrieved from `https://journals.ametsoc.org/view/journals/clim/18/21/jcli3539.1.xml` doi: 10.1175/JCLI3539.1

Årthun, M., Onarheim, I. H., Dörr, J., & Eldevik, T. (2021). The seasonal and regional transition to an ice-free arctic. *Geophysical Research Letters*, *48*(1), e2020GL090825. Retrieved from `https://agupubs.onlinelibrary.wiley.com/doi/abs/10.1029/2020GL090825` (e2020GL090825 2020GL090825) doi: https://doi.org/10.1029/2020GL090825

High-latitude stratospheric aerosol geoengineering can be more effective if injection is limited to spring: supplementary material

Walker Lee, Douglas G. MacMartin, Daniele Visioni, Ben Kravitz
Submitted January 2021

a. Table of climate values for MAM-60, ANN-60, and RCP8.5

Metric	**RCP8.5**	**MAM-60**	**ANN-60**
Global mean temperature (K)	289.18	-0.65 ± 0.06	-0.44 ± 0.06
Arctic mean temperature (K)	268.08	-3.7 ± 0.2	-2.5 ± 0.2
ITCZ, prcp. centroid method (deg. lat)	-0.21 ± 0.05	-0.3 ± 0.2	-0.17 ± 0.04
ITCZ, heat flux method (deg. lat)	-2.4 ± 0.1	-2.9 ± 0.1	-3.4 ± 0.1
SSI (million km^2)	0.32 ± 0.02	5.3 ± 0.1	2.9 ± 0.2
Total heat flux at 60°N (PW)	3.41 ± 0.01	3.45 ± 0.01	3.40 ± 0.02
Oceanic heat flux at 60°N (PW)	-1.4 ± 0.3	-1.3 ± 0.2	-1.5 ± 0.2
Atmospheric heat flux at 60°N (PW)	4.8 ± 0.3	4.9 ± 0.2	4.9 ± 0.2

This table presents values for various climate metrics discussed in the main text. All values are averaged over the years 2035-2039, which correspond to the last 5 years of simulation for MAM-60 and ANN-60. ± values indicate standard error. “Arctic mean temperature” refers to the average temperature north of 60°N. The ITCZ as defined by the precipitation centroid method refers to the centroid of precipitation between 20°S and 20°N. The ITCZ as defined by the heat flux method refers to the latitude of net zero meridional heat flux, found by fitting a linear function to meridional heat transport between 10°S and 10°N and finding the intercept. SSI refers to the extent of Northern Hemisphere sea ice during the month of September. Total heat flux is broken down into oceanic and atmospheric heat fluxes using the methods of Wunsch (2006).

b. AOD comparisons for injections at different latitudes, including MAM-30 and MAM-45

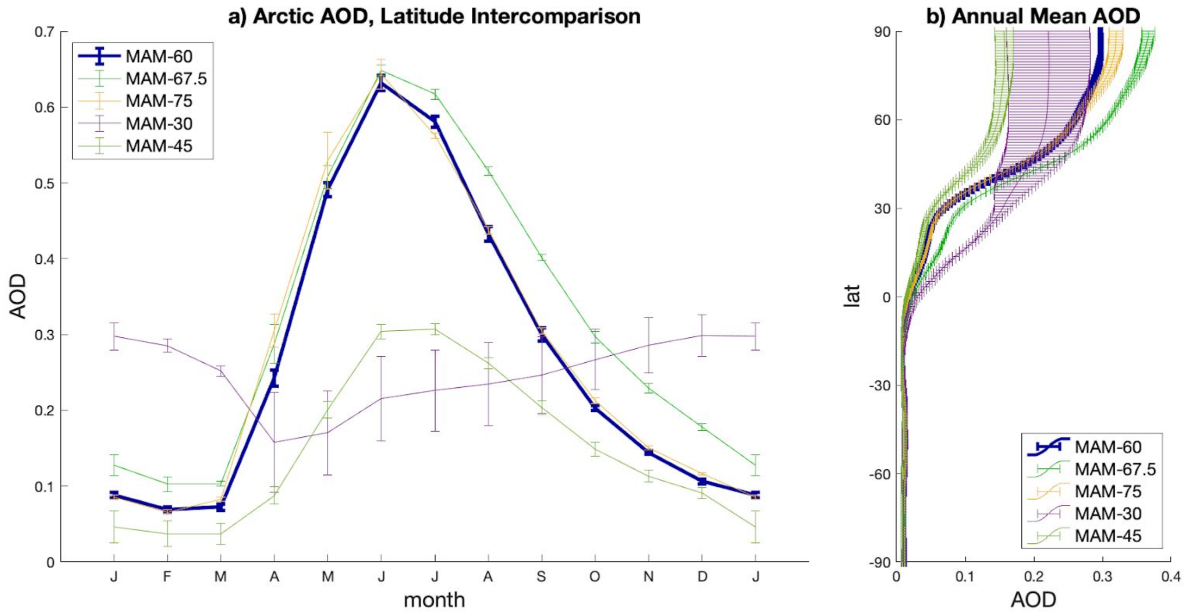

This figure presents Arctic AOD seasonal cycles and annual mean zonal mean AOD for MAM-60, MAM-67.5, and MAM-75 from this study alongside MAM-30 and MAM-45 from Visioni, MacMartin, Kravitz, Richter, et al. (2020). Data from MAM-60 is averaged over the last 5 years of simulation; all other data are averaged over the last 3 years of simulation.